Author/s:
Mao, W;Hall, CR;Chesman, ASR;Forsyth, C;Cheng, YB;Duffy, NW;Smith, TA;Bach, U

Title:
Visualizing Phase Segregation in Mixed-Halide Perovskite Single Crystals

Date:
2019-02-25

Citation:
Mao, W., Hall, C. R., Chesman, A. S. R., Forsyth, C., Cheng, Y. B., Duffy, N. W., Smith, T. A. & Bach, U. (2019). Visualizing Phase Segregation in Mixed-Halide Perovskite Single Crystals. Angewandte Chemie International Edition, 58 (9), pp.2893-2898. https://doi.org/10.1002/anie.201810193.

Persistent Link:
https://hdl.handle.net/11343/285298

Title: Visualizing Phase Segregation in Mixed-Halide Perovskite Single Crystals

Authors: Wenxin Mao, Masters; Christopher R. Hall, PhD; Anthony S. R. Chesman, PhD; Craig Forsyth, PhD; Yi-Bing Cheng, PhD; Noel W. Duffy, PhD; Trevor A. Smith; Udo Bach

To be cited as: 10.1002/anie.201810193

Link to VoR: https://doi.org/10.1002/anie.201810193

WILEY-VCH

Visualizing Phase Segregation in Mixed-Halide Perovskite Single Crystals

Wenxin Mao[†], Christopher R. Hall[†], Anthony S. R. Chesman, Craig Forsyth, Yi-Bing Cheng, Noel W. Duffy, Trevor A. Smith,* and Udo Bach*

Abstract: Mixed organolead halide perovskites (MOHPs), $CH_3NH_3Pb(Br_xI_{1-x})_3$, have been shown to undergo phase segregation into I-rich domains under illumination, presenting a major challenge to their development in photovoltaic and light-emitting devices. Recent work suggests phase segregated domains are localized at crystal boundaries, driving investigations into the role of edge structure and the growth of larger crystals with reduced surface area. Herein, a method for growing large (30×30×1 µm) monocrystalline $MAPb(Br_xI_{1-x})_3$ single crystals is presented. The direct visualization of the growth of nanocluster-like I-rich domains throughout the entire crystal revealed grain boundaries are not required for this transformation. Narrowband fluorescence imaging and time-resolved spectroscopy provided new insight into the nature of phase segregated domains and the collective impact on optoelectronic properties.

In recent years, $CH_3NH_3Pb(Br_xI_{1-x})_3$ ($MAPb(Br_xI_{1-x})_3$) MOHP polycrystalline thin films have garnered enormous interest for device applications due to a large absorption coefficient, long carrier lifetimes and diffusion length, and an insensitivity to structural defects [1]. While MOHPs offer bandgap energies that can be readily tuned by varying their Br:I ratio [2], visible light irradiation can induce the formation of iodide- and bromide-rich domains, a process commonly known as phase segregation [3]. The general aspects of phase segregation are well established. In particular, Hoke et al. showed that the characteristic feature of the light induced red-shift in the emission spectra of mixed- halide perovskites is accompanied by a splitting of X-ray diffraction peaks, suggesting the formation of two distinct domains and highlighting the structural origin of this effect.

Recent work has shown that phase segregation is mediated by halide ion diffusion between halide site vacancies [1a]. Such defects form throughout MOHPs due to a low activation energy [4], enabling ion migration to take place under certain conditions. For example, with an applied electric field, ion and vacancy migration has been linked to current-voltage hysteresis in devices [5]. The grain boundaries are also suspected of playing an important role, with faster ion migration observed at the boundaries compared with the grain interior [6], suggesting a fundamentally different environment exists at grain boundaries, consistent with fluorescence measurements [7]. Recent results utilising passivation suggests this may be due to a high-density of vacancies that exist at grain boundaries [8].

High-resolution imaging methods have yielded further insight into the structural interactions at play during light-induced phase segregation, with both Bischak et al. [9] and Tang et al [10] revealing that illumination caused iodide-enriched domains to form near interfaces between grain boundaries. Bischak suggested these domains migrate to grain boundaries to relieve strain within single grains, whilst Tang et al. suggested the positive space charge at the grain boundary interface attract I^- ions where they accumulate, yielding a localised I-rich composition.

These imaging experiments were carried out on polycrystalline perovskite films which exhibit high defect densities [11] and small grain sizes, presenting difficulties in isolating the role of defects and surface states in phase segregation. Furthermore, the grain size and 3-dimensional nature of polycrystalline films make it challenging to assign emissive features to edge states or the grain interior. In contrast, large area and thin monocrystalline perovskite microplatelets permit the study of phase segregation with optical imaging and spectroscopic techniques, allowing for the unambiguous interrogation of grain boundaries and grain interior regions. Recently, we demonstrated the use of precursor crystals that transform into monocrystalline $MAPbBr_3$ (pure-Br) microplatelets via a supersaturated solution intermediate [12]. Herein, we adapt this approach to grow thin (~1 µm) mixed-halide perovskite single crystals, which are used in the microspectroscopic study of phase segregation. Using a combination of confocal and widefield fluorescence microscopy methods, we visualize the formation and growth of position locked I-rich clusters throughout entire single crystals during illumination, in direct contrast to the recent work of Bischak [9] and Tang [10], providing new insight into the driving mechanisms. We use a combination of widefield narrowband fluorescence imaging and time-resolved fluorescence to gain new insight into the nature of these domains and their impact on optoelectronic properties.

Microplatelets of compositionally-uniform mixed-halide perovskites were grown by modifying an existing procedure [7]. In

[a] W. Mao, Prof. U. Bach
Department of Chemical Engineering, Monash University
Clayton, Victoria, Australia
E-mail: udo.bach@monash.edu
[b] W. Mao, Dr. C. Hall, Dr. A. Chesman, Prof. Y. Cheng, A/Prof. T. Smith, Prof. U. Bach
Australian Research Council Centre of Excellence in Exciton Science
[c] Dr. C. Hall, A/Prof. T. Smith
Department of Chemistry, Faculty of Science, University of Melbourne
Melbourne, Victoria, Australia
E-mail: trevoras@unimelb.edu.au
[d] Dr. A. Chesman,
, Clayton, Victoria, Australia
[e] Dr. A. Chesman, Prof. U. Bach
Melbourne Centre for Nanofabrication, Victoria, Australia.
[f] Dr. C. Forsyth
School of Chemistry, Monash University
Clayton, Victoria, Australia
[g] Prof. Y. Cheng
Department of Materials and Science Engineering, Monash University
Clayton, Victoria 3800, Australia
[h] Dr. N. Duffy
CSIRO Energy, Clayton, Victoria, Australia
[†] These authors contributed equally to this work
Supporting information for this article is given via a link at the end of the document.

brief, vapour diffusion into a solution containing lead bromide ($PbBr_2$), methylammonium bromide (MABr) and methylammonium iodide (MAI) in dimethylformamide (DMF) at 0 °C resulted in the crystallisation of (MA)[$PbBr_xI_{3-x}$]·DMF (Figure S1 and S2). The crystal structure of the material contains 1D chains of $PbBr_xI_{3-x}$, with the methylammonium cations and DMF solvent molecules residing in the lattice (Figure 1a). X-ray crystallography reveals halides occupy three unique positions, labelled as 1, 2 and 3 in Figure 1a, with I preferentially substituting for Br at positions 2 and 3. Compared to our recently reported 1D intermediate structure of pure $MAPbBr_3$·DMF, where parallel stacking of octahedra was observed, the introduction of I atoms leads to a mirrored octahedral stacking (Figure S3) [12,13]. The SEM image of the 1D crystals, Figure S4, indicates the structural uniformity of the fibres. Further details can be found in the Experimental Section and Figure S1 in the Supporting Information.

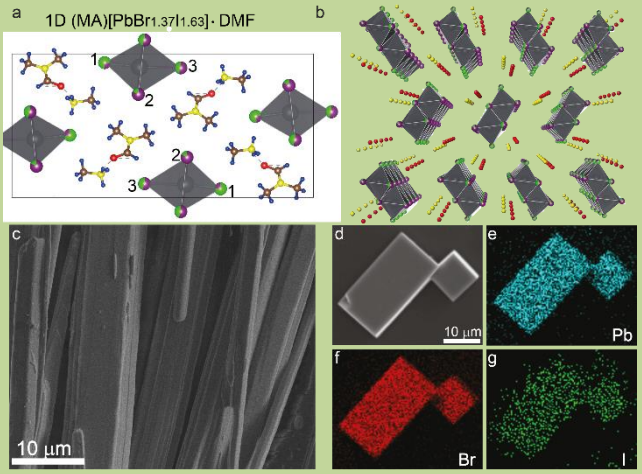

Figure 1. (a) Unit cell of (MA)[$PbBr_xI_{3-x}$]·DMF with the ratio of I:Br= 1.63:1.37 (Red spheres: oxygen atoms; brown spheres: carbon atoms; yellow spheres: nitrogen atoms; blue spheres: hydrogen atoms; purple spheres: iodine atoms; green spheres: bromine atoms; grey polyhedrons: PbX_6 octahedrons). (b) Crystal structure of (MA)[$PbBr_xI_{3-x}$]·DMF viewed down the crystallographic a-axis (red spheres: DMF molecules; yellow spheres: MA cations; black spheres: halide atoms; grey polyhedrons: PbX_6 octahedrons.) (c) Low temperature Scanning Electron Microscope (SEM) image of the 1D fibres. (d-g) SEM and EDS (Energy-dispersive X-ray spectroscopy) mapping of two $MAPb(Br_xI_{1-x})_3$ microplatelets.

Upon warming to room temperature, the DMF solvent molecules were lost from the lattice of the crystal and the material deliquesced, giving a supersaturated solution of precursor ions. As $MAPb(Br_xI_{1-x})_3$ began to nucleate from the solution, the remaining (MA)[$PbBr_xI_{3-x}$]·DMF dissolved to provide additional precursors for further growth of the mixed-halide microplatelets (Figure S5). At the conclusion of this process the remaining DMF was wicked away to terminate the crystal growth and prevent the $MAPb(Br_xI_{1-x})_3$ crystals redissolving in the excess solvent (Figure S6). The growth process was controlled to yield platelets with thicknesses ranging from a few hundred nanometres to a few microns with edge lengths of several tens to one hundred microns [7]. Powder X-ray diffraction (PXRD) was used to examine the structure of the product (Figure S7). The diffraction peaks move slightly towards lower diffraction angles with the incorporation of iodide, suggesting an enlarged lattice spacing originating from the replacement of Br by the larger radius I. The I:Br composition of the as-synthesized $MAPb(Br_xI_{1-x})_3$ crystal is between 1:9 to 2:8, as determined by comparing the absorption spectrum with spin coated $MAPb(Br_xI_{1-x})_3$ films (Figure S8a, b). Notably, different I:Br ratio in the final composition can be achieved with elevated temperatures (Figure S8c) due to the different nucleation energies of Br- and I-based perovskites.[14]

AFM (Figure S9), SEM (Figure 1d) and EDS mapping (Figure 1e-g) show clean single crystal microplatelets, with I and Br homogeneously distributed in the dark. More examples of EDS measurements on other crystals from various synthesized batches are shown in Figure S10 and S11. Dark-field PL images of single crystals show efficient emission waveguiding to the crystal boundary, in contrast to polycrystalline structures (Figure S12)[12], suggesting a high-quality single-crystal material.

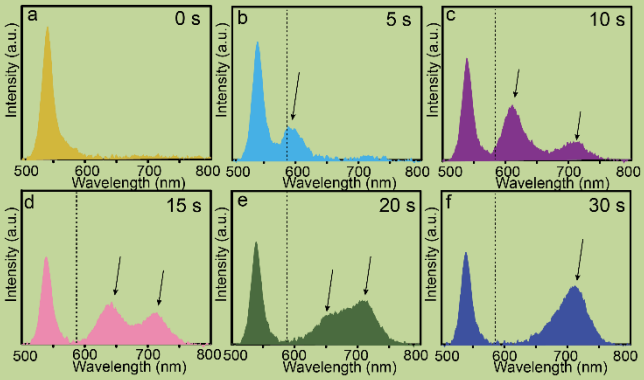

Figure 2. (a-f) Time-dependent fluorescence spectra of light-induced phase segregation recorded in the centre of a single $MAPb(Br_xI_{1-x})_3$ microplatelet recorded over 30 seconds with a confocal microscope at 294K. For excitation we used 400 nm pulsed laser with excitation intensity of 3.5 W cm^{-2}.

We first explored if phase segregation occurs in single crystal perovskites in an internal location far from the crystal edges, where phase segregation was reported to occur by Bischak and Tang[9, 10]. This was achieved through the use of a confocal microscope to excite and collect the emission spectra from the centre of single $MAPb(Br_xI_{1-x})_3$ microplatelet at 294 K. For excitation, 400 nm light (3.5 W cm^{-2}) generated from the second harmonic of a 800 nm Ti:sapphire 50 fs pulsed laser with repetition rate 2.7 MHz was used. Further details of the experimental apparatus are described in the SI and in Figure S13. Emission spectra were recorded from the centre of a single microplatelet in 1 second intervals with the key time intervals plotted in Figure 2 (full set shown in Figure S14). The data show complex and rapidly evolving emission spectra. Immediately following excitation, a single emission peak at 545 nm, typical of Br-rich-phase emission, was observed [9]. Continuous irradiation over 30 seconds caused the growth and decay of a central peak that monotonically red-shifted from 580 nm to 650 nm. This was accompanied by the growth of a broad peak at 700 nm, and the decrease of the Br-rich emission at 545 nm. Previous work has shown I-rich perovskites fluoresce around 700 nm, while the emission of mixed-halide MOHPs can be tuned between 545 nm and 760 nm by varying the Br:I ratio [3a, 15]. Significantly, the appearance of new emission peaks at wavelengths longer than 610 nm indicates the existence of domains where the I composition exceeds the as-grown I/Br ratio, which is consistent with phase segregation. We observe a similar appearance of I-rich emission for lower excitation intensities (115 $mWcm^{-2}$), however, no emission is captured from the Br-rich and intermediate bandgaps (Figure S15), suggesting photogenerated carriers are funnelled into and recombine in the

lower bandgap I-rich domains. As a control, time-dependent PL measurements were also carried on pure-Br and pure-I perovskites (Figure S16 and supplementary video 1), which revealed the observed features are indeed limited to MOHPs.

The accumulation of I into I-rich domains shown here occurred far from the crystal edges, suggesting grain boundaries and the associated defect states are not necessary for phase segregation. Interestingly, the synchronised growth of I-rich domains within the excitation region, as shown by a gradual shift in the mixed-halide phase, is notably different to the two-state-like evolution of two mixed-phase emission peaks observed in earlier phase segregation studies [3a, 9, 16]. It is posited that such a feature may be due to the highly homogeneous conditions present within the focal volume in the high-quality microplatelets, which leads to excited-state features that evolve at near uniform rates. After several minutes in the dark the sample returned to its unsegregated form (Figure S17).

To further investigate the nature of phase segregation we imaged the photoluminescence of single microplatelets with narrowband widefield fluorescence microscopy. Figure 3 shows a series of fluorescence images for a single microplatelet recorded

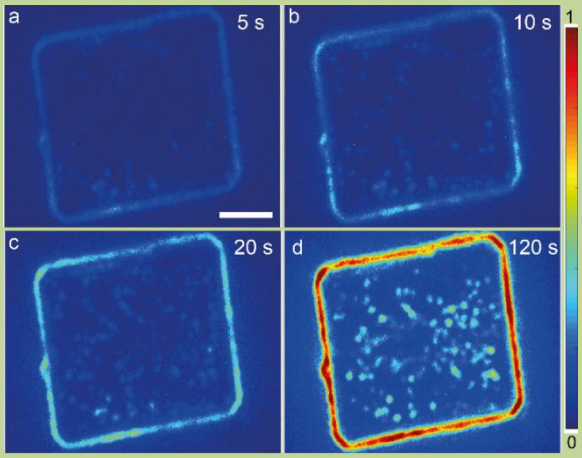

Figure 3. (a-d) Widefield photoluminescence images of a MAPb(Br_xI_{1-x})$_3$ single crystal collected over 120 s in the I-rich emission region (660–700 nm). Continuous blue light (400–450 nm, 5 mW cm^{-2}) was used as the excitation source. The scale bar is 5 µm.

at 680 nm (FWHM 45 nm). With continuous illumination by a halogen lamp, filtered to produce 400–450 nm light (5 mW cm^{-2}), small emissive features in the I-rich emission region appear within the grain boundary. Over 120 seconds, bright emission centres ~1 µm in size form throughout the crystal. The gradual appearance of emissive features at 680 nm is consistent with the growth of red-shifted emission from I-rich domains as shown in Figure 2, This is despite the low excitation intensity, highlighting the prevalence of this interaction in MOHPs. The growth of these features is also observed at higher excitation

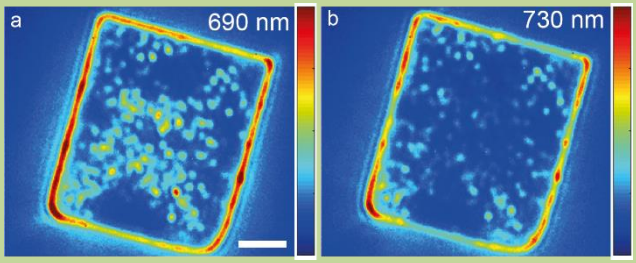

intensity (3.5 W cm^{-2}), as shown with confocal microscopy in Figure S19 (supplementary video 2). The formation of stable I-rich domains throughout microplatelets is in stark contrast to the work of Bischak et al. and Tang et al. on polycrystalline films [9, 10]. In this work we show unequivocally that grain boundaries are not an essential requirement for phase segregation. The appearance of these features in large single microplates therefore suggests efforts towards growing larger grains with a relative reduction in boundary interface area will not lessen the effects of phase segregation since I-rich domains form throughout the entire grain.

Figure 4. (a,b) Widefield microscopic PL images of a MAPb(Br_xI_{1-x})$_3$ single crystal after 10 min continuous illumination with 425 nm light (5 mWcm^{-2}). The wavelength regions are (a) 690±20 nm and (b) 730±20 nm. The scale bar is 5 µm.

Large MOHP microplates also present an opportunity to study the nature of individual phase segregated domains with conventional microspectroscopy techniques. We extend our investigation by collecting widefield fluorescence images of a single microplatelet centred at 690 and 730 nm, corresponding to the peak and red-edge emission of the I-rich domains, using a tuneable bandpass filter (Kurios-WB1, Thorlabs). Photoluminescence images, shown in Figure 4, are recorded after continuous excitation with 400–450 nm light at 5 mW cm^{-2} for 10 minutes. Both emission regions show strong waveguided emission at the edges of the platelet, while localised emission from I-rich domains is observed throughout. The most striking feature is that different I-rich domains are dominant in each spectral window. In the 690 nm emission window there are more I-rich domains in the centre of the platelet than at 730 nm. The observation of phase segregated domains with different emission spectra has not been shown previously. Significantly, this difference indicates the broad emission spectrum of phase segregated MOHPs comprises a distribution of domains with different I composition. Many processes could contribute to this difference, including a non-uniform distribution of non-radiative trap states, which may have a role in controlling I^- migration [17], or the availability of I^- in different regions due to the density of phase segregated domains, however, further work is required to clearly understand the origin.

It has also been suggested that I-rich domains migrate to grain boundaries to relieve strain [9], however, there is little time-dependent experimental evidence to support this claim. We used time dependent widefield imaging to track I-rich domain growth and position in real time over the entire single crystal (see Figure S20 and supplementary video 3). Under continuous excitation (5 mW cm^{-2}) we observe localised growth of I-rich domains (660–700 nm), however, there is no indication that the domains move during this time period. To further test the mobility of I-rich domains we exposed the microplatelet to multiple light-off (5 min) and light-on (3 min) cycles. Figure S21 shows widefield images taken over 4 cycles. After each cycle we find the I-rich domains form in the same locations, suggesting there is a structural feature promoting the formation of these domains in fixed locations, which would likely inhibit migration. These features are within 100-200 nm (160-330 unit cells) of the surface due to the limited penetration depth of the incident light.[18]

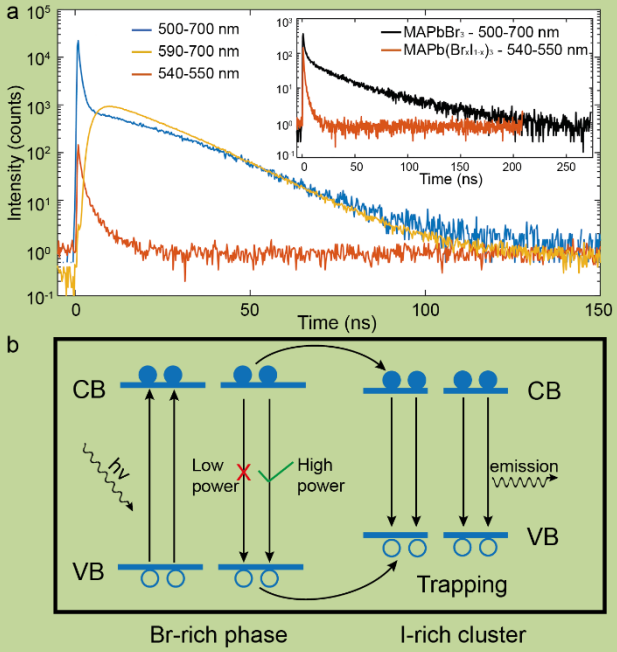

Figure 5. (a) Time-resolved fluorescence profiles measured at the centre of a single MAPb(Br_xI_{1-x})$_3$ microplatelet after light soaking. Plotted are the kinetics measured for the spectral region 500 to 700 nm (blue); the Br-rich region, 540–565 nm (orange); and the I-rich region, 610–700 nm (yellow). Inset: Comparison between kinetics measured for a $MAPbBr_3$ single crystal and the Br-rich emission from a MAPb(Br_xI_{1-x})$_3$ microplatelet. (b) Schematic illustrating carrier trapping and recombination in I-rich domains under continuous irradiation.

To elucidate the role of I-rich domains on the excited state dynamics we performed Time-Correlated Single Photon Counting (TCSPC) measurements on a single MOHP microplatelet. This is achieved using a confocal microscope, with 400 nm pulsed excitation (3.5 W cm^{-2}) and a single-photon counting PMT. Fluorescence dynamics were measured after 2 mins of continuous laser irradiation and are shown in Figure 5a. The blue line shows the emission dynamics for the full emission spectrum (500–700 nm). The shape of the curve is complex, with fast and slow features, with the slow component appearing to decay at multiple rates. Separately recoding the Br-rich (orange) and I-rich (red) spectral windows allowed for a deconvolution of the kinetics associated with each region; the Br-rich component decayed rapidly within the first 20 ns, with the I-rich component rising on the same time scale, followed by a multi-exponential decay. The sum of these two kinetic traces approximates the full spectrum dynamics given, indicating the key decay features are captured in the two selected emission windows.

In the inset we compare the emission kinetics for the Br-rich emission and the kinetics measured for a pure-Br single crystal. These have amplitude-weighted average lifetimes of 1.4 ns and 6.7 ns respectively, revealing the former is highly perturbed by the formation of I-rich domains. The rapid decay of the Br-rich emission, matched by a rise in the I-rich emission, is characteristic of a charge trapping process, where excited charge carriers are rapidly funnelled to low-bandgap I-rich domains where they are held until recombination. TCSPC measurements on pure $MAPbI_3$ (Figure S22) after light soaking indicate the delayed rise is a feature of MOHPs. These interactions can be described via a simple four-state model shown in Figure 5b. We suggest excitation in the high-bandgap Br-rich phase generates highly-mobile free electrons and holes, however, in a phase segregated MOHP, the low-bandgap I-rich domains trap excited carriers. The estimated conduction band energies for $MAPbI_3$ and $MAPbBr_3$ vary by only 0.09 eV [3b, 19], with the remaining difference in bandgap energy due to a vastly larger offset in the valence band energy. The large barrier in the valence band of I-rich domains (~200 meV) would be the major energy barrier for holes to move from the I-rich phase back to Br-rich areas. This suggests highly immobile holes trapped in I-rich domains are likely to be the primary process driving cluster localized emission.

From the perspective of devices, the instability of the MOHP bandgap arising from light-driven phase segregation presents a major challenge. Given the great potential of mixed-halide perovskites for optoelectronic device applications [8, 20], further investigation into understanding and controlling light induced phase segregation will be required. Recent work incorporating potassium halide into the growth of MOHP films [8] shows enormous promise for improving MOHP stability, however, it is clear from this work that any approach employed to address phase segregation must also target ion migration throughout the crystal, not just surface states.

In summary, we fabricated compositionally-uniform mixed-halide MAPb(Br_xI_{1-x})$_3$ perovskite single crystals through a dissolve-and-crystallize process. With this new material we directly visualize the light-induced formation of I-rich domains in mixed halide perovskites due to the phase segregation effect. Fixed I-rich domains are observed to form throughout large MAPb(Br_xI_{1-x})$_3$ microplatelets, in contrast to recent observations near grain boundaries in smaller grains of polycrystalline films. Spectrally selective fluorescence microscopy reveals variation between I-rich domains, suggesting fluctuations in domain composition contribute to the broad emission spectra for phase segregated MOHPs. Time-resolved fluorescence measurements show the low bandgap I-rich domains efficiently trap free-carriers, revealing their dominant role as radiative recombination centres. The ability to study phase segregation in large single microplatelets provides an excellent platform to study the optoelectronic properties of perovskites, whilst perovskite microplatelets also present new opportunities for expanding the

functional applications of mixed halide perovskites in sensing, switching, or memory applications.

Experimental Section

Experimental Details are provided in Supporting Information

Acknowledgements

This work was financially supported by Australian Research Council Centre of Excellence in Exciton Science. We gratefully acknowledge financial support from the Australian Government through the Australian Renewable Energy Agency and the Australian Centre for Advanced Photovoltaics, CSIRO through their OCE Science Leader Fellowship program (CE170100026 and DP160104575). We also acknowledge Prof. Paul Mulvaney, Dr. Asaph Widmer-Cooper, Dr. Stefano Bernardi and Dr. Weijian Chen for useful discussions. We also acknowledge use of the facilities and the assistance of Dr. Amelia Liu at the Monash Centre for Electron Microscopy.

Keywords: perovskite • single crystal • phase segregation • photoluminescence • lifetime

[1] a) A. Ruth, M. C. Brennan, S. Draguta, P. V. Kamat, M. Kuno, *ACS Energy Lett.* **2018**, 3, 204-213; b) S. D. Stranks, G. E. Eperon, G. Grancini, C. Menelaou, M. J. P. Alcocer, T. Leijtens, L. M. Herz, A. Petrozza, H. J. Snaith, *Science* **2013**, 342, 341-344; c) Z.-K. Tan, R. S. Moghaddam, M. L. Lai, P. Docampo, R. Higler, F. Deschler, M. Price, A. Sadhanala, L. M. Pazos, D. Credgington, F. Hanusch, T. Bein, H. J. Snaith, R. H. Friend, *Nat. Nanotechnol* **2014**, 9, 687; d) H. Zhu, Y. Fu, F. Meng, X. Wu, Z. Gong, Q. Ding, M. V. Gustafsson, M. T. Trinh, S. Jin, X. Y. Zhu, *Nat. Mate* **2015**, 14, 636; e) Q. Dong, Y. Fang, Y. Shao, P. Mulligan, J. Qiu, L. Cao, J. Huang, *Science* **2015**, 347, 967-970.

[2] a) J. H. Noh, S. H. Im, J. H. Heo, T. N. Mandal, S. I. Seok, *Nano Lett.* **2013**, 13, 1764-1769; b) S. R. J., E. G. E., M. Laura, P. E. S., K. B. A., P. J. B., H. M. T., J. M. B., H. A. Abbas, M. D. T., S. H. J., *Adv Energy Mater.* **2016**, 6, 1502458.

[3] a) E. T. Hoke, D. J. Slotcavage, E. R. Dohner, A. R. Bowring, H. I. Karunadasa, M. D. McGehee, *Chem. Sci.* **2015**, 6, 613-617; b) S. Draguta, O. Sharia, S. J. Yoon, M. C. Brennan, Y. V. Morozov, J. S. Manser, P. V. Kamat, W. F. Schneider, M. Kuno, *Nat. Commun.* **2017**, 8, 200.

[4] W. S. Yang, B.-W. Park, E. H. Jung, N. J. Jeon, Y. C. Kim, D. U. Lee, S. S. Shin, J. Seo, E. K. Kim, J. H. Noh, S. I. Seok, *Science* **2017**, 356, 1376-1379.

[5] C. Eames, J. M. Frost, P. R. F. Barnes, B. C. O'Regan, A. Walsh, M. S. Islam, *Nat. Commun.* **2015**, 6, 7497.

[6] J. S. Yun, J. Seidel, J. Kim, A. M. Soufiani, S. Huang, J. Lau, N. J. Jeon, S. I. Seok, M. A. Green, A. Ho-Baillie, *Adv Energy Mater.* **2016**, 6, 1600330.

[7] D. W. de Quilettes, S. M. Vorpahl, S. D. Stranks, H. Nagaoka, G. E. Eperon, M. E. Ziffer, H. J. Snaith, D. S. Ginger, *Science* **2015**, 348, 683-686.

[8] M. Abdi-Jalebi, Z. Andaji-Garmaroudi, S. Cacovich, C. Stavrakas, B. Philippe, J. M. Richter, M. Alsari, E. P. Booker, E. M. Hutter, A. J. Pearson, S. Lilliu, T. J. Savenije, H. Rensmo, G. Divitini, C. Ducati, R. H. Friend, S. D. Stranks, *Nature* **2018**, *555*, 497.

[9] C. G. Bischak, C. L. Hetherington, H. Wu, S. Aloni, D. F. Ogletree, D. T. Limmer, N. S. Ginsberg, *Nano Lett.* **2017**, 17, 1028-1033.

[10] X. Tang, M. van den Berg, E. Gu, A. Horneber, G. J. Matt, A. Osvet, A. J. Meixner, D. Zhang, C. J. Brabec, *Nano Lett.* **2018**, 18, 2172-2178.

[11] a) trapp b) Q. Dong, Y. Fang, Y. Shao, P. Mulligan, J. Qiu, L. Cao, J. Huang, *Science* **2015**, *347*, 967-970.

[12] M. Wenxin, Z. Jialu, Z. Yupeng, C. A. S. R., O. Qingdong, H. Jamie, L. Feng, W. Ziyu, G. Brenton, B. T. D. M., R. M. Uller, D. N. W., S. Leone, C. Yi-Bing, B. Qiaoliang, B. Udo, *Angew. Chem. Int. Ed.* **2017**, 56, 12486-12491.

[13] Y. Guo, K. Shoyama, W. Sato, Y. Matsuo, K. Inoue, K. Harano, C. Liu, H. Tanaka, E. Nakamura, *J. Am. Chem. Soc.* **2015**, 137, 15907-15914.

[14] L. Wang, G. D. Yuan, R. F. Duan, F. Huang, T. B. Wei, Z. Q. Liu, J. X. Wang, J. M. Li, *AIP Adv.* **2016**, *6*, 045115.

[15] A. J. Barker, A. Sadhanala, F. Deschler, M. Gandini, S. P. Senanayak, P. M. Pearce, E. Mosconi, A. J. Pearson, Y. Wu, A. R. Srimath Kandada, T. Leijtens, F. De Angelis, S. E. Dutton, A. Petrozza, R. H. Friend, *ACS Energy Lett.* **2017**, 2, 1416-1424.

[16] D. J. Slotcavage, H. I. Karunadasa, M. D. McGehee, *ACS Energy Lett.* **2016**, 1, 1199-1205.

[17] D. W. deQuilettes, W. Zhang, V. M. Burlakov, D. J. Graham, T. Leijtens, A. Osherov, V. Bulović, H. J. Snaith, D. S. Ginger, S. D. Stranks, *Nat. Commun.* **2016**, *7*, 11683.

[18] a) A. M. A. Leguy, P. Azarhoosh, M. I. Alonso, M. Campoy-Quiles, O. J. Weber, J. Yao, D. Bryant, M. T. Weller, J. Nelson, A. Walsh, M. van Schilfgaarde, P. R. F. Barnes, *Nanoscale* **2016**, *8*, 6317-6327; b) B. Wenger, P. K. Nayak, X. Wen, S. V. Kesava, N. K. Noel, H. J. Snaith, *Nat. Commun* **2017**, *8*, 590.

[19] a) K. T. Butler, J. M. Frost, A. Walsh, *Mater Horizons* **2015**, 2, 228-231; b) S. A. Bretschneider, J. Weickert, J. A. Dorman, L. Schmidt-Mende, *APL Mater.* **2014**, 2, 040701.

[20] D. P. McMeekin, G. Sadoughi, W. Rehman, G. E. Eperon, M. Saliba, M. T. Hörantner, A. Haghighirad, N. Sakai, L. Korte, B. Rech, M. B. Johnston, L. M. Herz, H. J. Snaith, *Science* **2016**, 351, 151-155.

WILEY-VCH

Entry for the Table of Contents (Please choose one layout)

COMMUNICATION

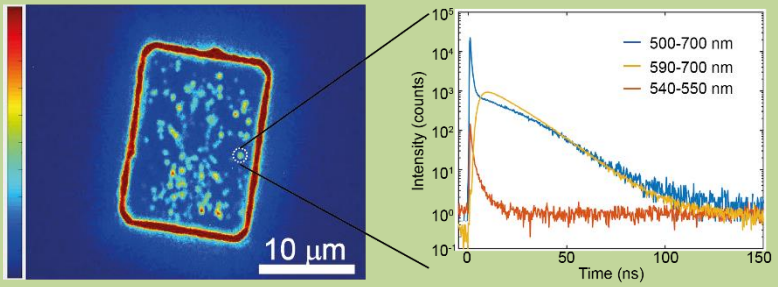

Wenxin Mao, Christopher Hall Anthony S. R. Chesman, Craig Forsyth, Yi-Bing Cheng, Noel W. Duffy, Trevor A. Smith, and Udo Bach**

Visualizing Phase-Segregation in Mixed-Halide Perovskite Single Crystals

Iodide-rich clusters form and grow in the $MAPb(Br_xI_{1-x})_3$ single crystal with continuous light illumination. A combination of widefield microscopy and confocal microscopy provides detailed insight into phase segregation in individual $MAPb(Br_xI_{1-x})_3$ microplatelets.